Characterization of Numerical Dissipation Rates in Numerical Simulations Performed Using Discontinuous Galerkin Methods

**By G. Castiglioni, J.A. Domaradzki, N. Krais†, A. Beck†, C.-D. Munz†
AND F. Schranner‡**

Department of Aerospace Engineering
University of Southern California
Los Angeles, CA 90089-1191, U.S.A.

Recently it has become increasingly clear that the role of a numerical dissipation, originating from the discretization of governing equations of fluid dynamics, rarely can be ignored while using explicit or implicit Large Eddy Simulations (LES). The numerical dissipation inhibits the predictive capabilities of LES whenever it is of the same order of magnitude or larger than the subgrid-scale (SGS) dissipation. This situation is generally encountered in LES performed with lower order finite volume (FV) [1] or finite difference (FD) [2] numerical methods. However, it is expected that numerical dissipation effects are negligible when high order methods are employed. One of such methods is the Discontinuous Galerkin Spectral Element Method (DGSEM) that can be regarded as a hybrid FV and Finite Elements (FE) method [3]. The purpose of this work is a systematic analysis of the numerical dissipation in the DGSEM method implemented in the code FLEXI developed by the Numerics Research Group at Stuttgart University. The analysis uses the procedure proposed recently by [1] that allows to compute the numerical dissipation rate and numerical viscosity in the physical space for arbitrary sub-domains in a self-consistent way, using only information provided by the code in question. The procedure is implemented for a three-dimensional Taylor-Green vortex (TGV) flow simulated using the DG method and compared with results obtained previously for the same flow using a FV code.

1. Introduction

Direct Numerical Simulations (DNS) of turbulent flows are excessively computationally expensive for complex geometries and/or high Reynolds number flows due to the wide separation of physical scales that need to be resolved. A relatively successful way to reproduce the dynamics of Navier-Stokes (N-S) equations while reducing the number of degrees of freedom is the Large Eddy Simulations (LES) approach. In LES the number of degrees of freedom is reduced by means of a spatial filter that suppresses the effects of small scales at the cost of introducing subgrid scale (SGS) unknowns (i.e. for the incompressible N-S the SGS stress tensor) which must be explicitly modeled [4–6].

† Institut für Aerodynamik und Gasdynamik, Universität Stuttgart, Pfaffenwaldring 21, 70569 Stuttgart
‡ Lehrstuhl für Aerodynamik und Strömungsmechanik, Technische Universität München, Boltzmannstr. 15, 85748 Garching b. München

An alternative approach is to use the numerical dissipation coming from the discretization of the N-S equations as an implicit LES (ILES) model. The strategy of using the truncation error as implicit model dubbed monotonically integrated LES (MILES) originated with the idea of [7] and is reviewed by [8]. MILES approach has been controversial and as such it has been subject of several investigations [9,10]. These studies have not been particularly encouraging. Even when MILES appears to reproduce qualitatively the dynamics of N-S equations a more in depth, quantitative investigation has shown that this is not the case. [9] showed that the numerical dissipation in a low order compressible solver is excessive with respect to the correct SGS dissipation leading to poor results both in ILES and explicit LES (ELES) configuration. However, in the modeling community relying on the numerical dissipation in place of explicit SGS models is becoming more and more popular. Such simulations are often called ILES though a more proper name should be under-resolved DNS (UDNS). The reason for this trend and the attractiveness of the approach is its simplicity, the lack of a universal explicit SGS model, and a qualitative behavior that mimics the dynamics of N-S equations. Furthermore UDNS simulation often are validated with experimental results which themselves suffer from high degree of uncertainty.

In order to mitigate the numerical dissipation effects in LES high order numerical methods should be used. The most common among high order methods are pseudo-spectral Fourier and Chebyshev methods but their use is restricted to simple geometries, e.g., a triply periodic box or channel and Blasius boundary layer flows. The Discontinuous Galerkin Spectral Element Methods (DGSEM) offer a high order alternative for simulating fluid flows in complex geometries [3]. However, the presence of discontinuities at the elements' boundaries and sometimes use of filtering to stabilize simulations [11] may introduce the numerical dissipation into a system. While it is expected that the numerical dissipation in the DGSEM methods is negligible it is important to establish quantitatively that this is indeed the case. The purpose of this work is a systematic analysis of the numerical dissipation in the DGSEM method implemented in the code FLEXI developed by the Numerics Research Group at Stuttgart University. The analysis uses the procedure proposed recently in [1] that allows to compute the numerical dissipation rate and numerical viscosity in the physical space for arbitrary sub-domains in a self-consistent way, using only information provided by the code in question, in this case FLEXI. The procedure is implemented for a three-dimensional Taylor-Green vortex (TGV) flow simulated using the DG method and compared with results obtained previously for the same flow using a FV code.

2. Equations and the Procedure for Estimating Numerical Dissipation

Analytical Form

Transport energy equation for compressible Navier-Stokes (N-S) is

$$\frac{\partial \rho e}{\partial t} + \frac{\partial}{\partial x_j}\left[\left(\rho e + p\right) u_j\right] = \frac{\partial u_i \tau_{ij}}{\partial x_j} - \frac{\partial q_j}{\partial x_j}, \tag{2.1}$$

where u_i are the components of the velocity vector, p the pressure, ρ the density and e the total energy per unit mass. The constitutive relation between stress and strain rate for a Newtonian fluid is

$$\tau_{ij} = \mu\left[\left(\frac{\partial u_i}{\partial x_j} + \frac{\partial u_j}{\partial x_i}\right) - \frac{2}{3}\frac{\partial u_k}{\partial x_k}\delta_{ij}\right], \tag{2.2}$$

the heat flux q_i is defined as

$$q_i = -k\frac{\partial T}{\partial x_i},\tag{2.3}$$

where μ is the dynamic viscosity, k is the thermal conductivity, and T is the temperature. The definition of total energy is

$$e = e^{in} + e^{kin},\tag{2.4}$$

where e^{in} is the specific energy per unit mass and $e^{kin} = \frac{1}{2}u_i u_i$ the kinetic energy. Following the procedure of [1] the transport equation, Eq. (2.1), can be separated into the contribution of internal energy

$$\frac{\partial \rho e^{in}}{\partial t} + \frac{\partial \rho e^{in} u_j}{\partial x_j} = -p\frac{\partial u_j}{\partial x_j} + \tau_{ij}\frac{\partial u_i}{\partial x_j} - \frac{\partial q_j}{\partial x_j},\tag{2.5}$$

and kinetic energy

$$\frac{\partial \rho e^{kin}}{\partial t} + \frac{\partial \rho e^{kin} u_j}{\partial x_j} = -u_j\frac{\partial p}{\partial x_j} + u_i\frac{\partial \tau_{ij}}{\partial x_j}.\tag{2.6}$$

After some manipulations the integral form of Eq. (2.6) can be written as

$$\frac{\partial}{\partial t}\int_V \rho e^{kin}dV + \int_A \left(\rho e^{kin}u_j + u_j p - u_i \tau_{ij}\right)n_j dA$$

$$+ \int_V \left(-p\frac{\partial u_j}{\partial x_j} + \tau_{ij}\frac{\partial u_i}{\partial x_j}\right)dV =$$

$$\frac{\partial}{\partial t}E^{kin} + F^{kin} + F^{ac} - F^{vis} - W^p + \varepsilon^{vis} = 0,\tag{2.7}$$

where F^{kin}, F^{ac}, F^{vis} are the kinetic energy, acoustic and viscous fluxes, n_j the outward unit vector normal to the surface A, W^p the work due to pressure and ε^{vis} the viscous dissipation. Notice that in the incompressible limit $W^p = 0$ as $\partial u_j/\partial x_j = 0$.

We can define a dissipation function ε as

$$\varepsilon = \int_V \frac{1}{\nu}\tau_{ij}\frac{\partial u_i}{\partial x_j}dV,\tag{2.8}$$

therefore $\varepsilon\nu = \varepsilon^{vis}$, where ν is the kinematic viscosity ($\nu = \mu/\rho$). Note that the above equation is exact only if $\nu = const$ in V.

2.1. *Discretized Form*

The method for quantifying the numerical dissipation was originally developed to analyze flow fields obtained from a FV code [1]. If we assume a FV spatial discretization and generic discretization in time then the Eq. (2.7) is contaminated by the truncation and aliasing errors and we can define a local residual

$$-\varepsilon^n_{(m)} = \frac{\Delta E^{kin}_{(m)}}{\Delta t} + F^{kin}_{(m)} + F^{ac}_{(m)} - F^{vis}_{(m)} - W^p_{(m)} + \varepsilon^{vis}_{(m)},\tag{2.9}$$

where the subscript $[\ \ ]_{(m)}$ refers to the mth control volume. We call the residual ε^n a numerical dissipation rate because it has been shown that if integrated over a sufficiently large control volume it has a predominantly dissipative character [1, 12]. This is also accounted for by a negative sign on the l.h.s. of the definition (2.9) so that ε^n itself is

positive as is the viscous dissipation ε^{vis}. Following this definition we can recover the numerical kinematic viscosity as

$$\nu^n_{(m)} = \frac{\varepsilon^n_{(m)}}{\varepsilon_{(m)}}. \tag{2.10}$$

We can extend the above definitions to a sub-domain or to the entire computational domain

$$\varepsilon^n_{sub} = \sum_m^M \varepsilon^n_{(m)} \quad ; \quad \nu^n_{sub} = \frac{\varepsilon^n_{sub}}{\varepsilon_{sub}}, \tag{2.11}$$

where M is total number of adjacent cells of a given sub-domain. For the latter, and in the incompressible limit, we can define the effective (or total) dissipation as

$$\varepsilon^{eff} = \varepsilon^{vis} + \varepsilon^n = -\frac{dE^{kin}}{dt}. \tag{2.12}$$

2.2. *Procedure*

Originally the procedure was developed to analyze a TGV flow simulated in a triply periodic domain on a uniform mesh in each Cartesian direction. To use the developed analysis tool the results of DG simulations have to be interpolated from nonuniform DG meshes to uniform meshes required by the tool. Kinetic fluxes in Eq. (2.9) are calculated as follows

$$F^{kin}_{(m)} = \left(\sum_r (\rho e^{kin} u_j n_j)_{(r)} \Delta A_{(r)} \right)_{(m)}, \tag{2.13}$$

where subscript $[\ \ ]_{(r)}$ represents the sum over the rth face of the mth control volume and $\Delta A_{(r)}$ is the area of the rth face. The other fluxes are computed in a similar fashion. Volume terms are calculated as (for example the kinetic energy)

$$E^{kin}_{(m)} = \left(\frac{1}{2} \rho u_i u_i \right)_{(m)} \Delta V_{(m)}, \tag{2.14}$$

where $\Delta V_{(m)}$ is the volume of the mth control volume. Note that if we take a periodic box the contribution of flux terms cancels out. For the time discretization for $\frac{\Delta E^{kin}_{(m)}}{\Delta t}$ a second-order three-points finite difference formula is used.

For the infinite Re number limit the viscous terms in Eq. (2.9) are dropped. In the incompressible limit ($Ma < 0.3$) the work due to pressure should be zero but this is not the case if the flow field is not exactly divergence free (as it can happen with compressible codes).

3. Numerical method

3.1. *The Discontinuous Galerkin Spectral Element Method*

FLEXI uses the Discontinuous Galerkin Spectral Element Method (DGSEM) to discretize the compressible Navier-Stokes equations (NSE). They read in conservation form

$$U_t + \nabla_x \cdot \mathbf{F}(U, \nabla_x U) = 0, \tag{3.1}$$

where U denotes the vector of conserved quantities $U = (\rho, \rho u_1, \rho u_2, \rho u_3, \rho e)^T$, the subscript t the time derivative and ∇_x the gradient operator in physical space. The flux

is split into advection and viscous fluxes, $\mathbf{F} = \mathbf{F}^a(U) - \mathbf{F}^v(U, \nabla_x U)$, and they read as

$$F_l^a(U) = \begin{pmatrix} \rho\, u_l \\ \rho\, u_1 u_l + \delta_{1l}\, p \\ \rho\, u_2 u_l + \delta_{2l}\, p \\ \rho\, u_3 u_l + \delta_{3l}\, p \\ \rho\, e u_l + p\, u_l \end{pmatrix}, \; F_l^v(U, \nabla_x U) = \begin{pmatrix} 0 \\ \tau_{1l} \\ \tau_{2l} \\ \tau_{3l} \\ \tau_{lj} u_j - q_l \end{pmatrix} \qquad (3.2)$$

with $l = 1, 2, 3$. The definitions of the viscous stresses τ_{ij} and the heat fluxes q_i can be found in Eq. (2.2) and Eq. (2.3), respectively. The viscosity coefficient μ, the Prandtl number Pr, the adiabatic exponent $\kappa = \frac{c_p}{c_v}$ with the specific heats c_p, c_v depend on the fluid and are taken as constant in this work. To close the system of equations, the perfect gas law

$$p = \rho R T = (\kappa - 1)\rho(e - \frac{1}{2}u_i u_i), \quad e = \frac{1}{2}u_i u_i + c_v T \qquad (3.3)$$

is used.

In order to solve the system of equations, the computational domain is subdivided into non-overlapping hexahedral elements, which we allow to be connected in a fully unstructured, but conforming way. We transform the NSE in a first step to a reference element $E \in [-1, 1]^3$. The associated mapping function $\mathbf{x}(\xi)$ is used to calculate the Jacobian $J(\xi) = \frac{\partial \mathbf{x}}{\partial \xi}$. How to construct the metrics while ensuring the so called free-stream preserving property is shown by Kopriva in [13]. Applying the transformation to the NSE in conservation form (3.1) leads to

$$J(\xi)\, U_t + \nabla_\xi \cdot \mathcal{F}(U, \nabla_x U) = J(\xi)\, U_t + \nabla_\xi \cdot (\mathcal{F}^{\mathbf{a}}(U) - \mathcal{F}^{\mathbf{v}}(U, \nabla_x U)) = 0, \qquad (3.4)$$

with the transformed fluxes $\mathcal{F}$. In the next step a tensor product of 1-D Lagrange polynomials ℓ^N of degree N is employed to express the discrete approximate solution vector as

$$U(\xi, t) = \sum_{i,j,k=0}^{N} \hat{U}_{ijk}(t)\psi_{ijk}^N(\xi), \qquad \psi_{ijk}^N(\xi) = \ell_i^N(\xi^1)\ell_j^N(\xi^2)\ell_k^N(\xi^3), \qquad (3.5)$$

where $\hat{U}_{ijk}(t)$ are the time dependent nodal degrees of freedom in each element. Following Kopriva [14], we choose the $N+1$ Gauss-Legendre quadrature points $\{\xi_i\}_{i=0}^N$ as interpolation nodes. Analogously, the discrete transformed flux $\mathcal{F}$ reads as

$$\mathcal{F}^l(U(\xi, \nabla_x U(\xi))) \approx \sum_{i,j,k=0}^{N} \hat{\mathcal{F}}_{ijk}^l \psi_{ijk}^N(\xi), \quad l = 1, 2, 3. \qquad (3.6)$$

We are going to derive the weak formulation in the next step. Multiplying Eq. (3.4) by a test function $\phi(\xi)$ and integrating over the reference element leads to

$$\int_E (J U_t + \nabla_\xi \cdot \mathcal{F}(U, \nabla_x U))\, \phi(\xi)\, d\xi = 0. \qquad (3.7)$$

Following the Galerkin approach the test functions are chosen identical to the basis functions in Eq. (3.5). Integration by parts yields the weak formulation

$$\frac{\partial}{\partial t} \int_E J U \phi\, d\xi + \oint_{\partial E} (\mathcal{F}_n^{a*} - \mathcal{F}_n^{v*})\, \phi\, ds - \int_E \mathcal{F}(U, \nabla_x U) \cdot \nabla_\xi \phi\, d\xi = 0, \qquad (3.8)$$

where $\mathcal{F}_n^{a*}$ denotes the numerical flux function normal to the surface for the inviscid terms, given by $\mathcal{F}_n^{a*} := \mathcal{F}_n^*(U^+, U^-)$ and superscripts $\pm$ denote the values at the grid cell interface from the neighbor and the local grid cell, respectively. For the inviscid numerical flux we can choose from several approximate Riemann solvers, see e.g. [15] for an overview. In this work the Roe, HLLC and local Lax-Friedrichs numerical flux functions were used. The numerical flux function for the viscous terms is denoted by $\mathcal{F}_n^{v*}$, resulting from the viscous flux $\mathcal{F}^v$ in Eq. (3.4). Through this viscous flux, Eq. (3.8) depends on the solution gradient $\nabla_x U$. Since the local gradients of the DG polynomial are not well suited to compute the viscous fluxes at the cell interfaces due to the discontinuous approximation, we use the first method by Bassi and Rebay [16], usually labeled BR1, to approximate the numerical viscous flux. This procedure is commonly referred to as lifting. We use a collocation approach and integrate Eq. (3.8) by Gauss quadrature in space on the same nodes used for interpolation. When we apply the numerical integration a semi discrete form is obtained, that is advanced in time by the fourth order accurate explicit Runge-Kutta method of Carpenter and Kennedy [17].

3.2. *Polynomial de-aliasing*

In Eq. (3.6) the nodal fluxes are evaluated on $N+1$ Gauss-Legendre quadrature points, which means that polynomials of degree $2N+1$ are integrated exactly. Since the flux functions $\mathcal{F}$ are non-linear, an additional error due to aliasing is introduced and can lead to stability issues for underresolved turbulent flows. For low-order DGSEM approximations, the inherent numerical deficiencies like dissipation errors will often lead to stable but inaccurate results. By increasing the polynomial degree these errors will be reduced and the resulting discretization will be more sensitive to aliasing, so an additional stabilization technique must be employed [18]. One approach to stabilization is to directly tackle the insufficient integration precision by use of a higher amount of integration points, so-called polynomial de-aliasing [19] or over integration. A straight forward way to implement this technique into the DGSEM framework is to use a sharp modal cutoff filter. The overintegrated calculation is then performed with a polynomial degree of $N_{over} > N$, and the approximate solution is filtered in every Runge-Kutta stage before the spatial residuals are evaluated to contain only the first $N+1$ modes. Kirby and Karniadakis [19] showed that de-aliasing for polynomial spectral methods is achieved by choosing $N_{over} = 2N$ for triple and $N_{over} = \frac{3}{2}N$ for quadratic non-linear integrands. Since the test cases in this work are nearly incompressible and the non-linearities in the flux functions for the incompressible NSE are quadratic, we choose $N_{over} = \frac{3}{2}N$ for the calculations presented here.

4. Results

The Taylor Green Vortex (TGV) flow originally described in [20] is chosen as a test case. This is the same test case that was used previously to validate the procedure applied to a research code INCA that implements the ALDM method as an implicit LES model [1, 21] and for the analysis of numerical dissipation in a commercial code Star-

Name	Elements	N	N_{Over}	Flux	Re
N31_OINT_Re#	2^3	31	47	LF	$3000, 1600, 800$
N15_OINT_Re#	4^3	15	23	LF	$3000, 1600, 800$
N7_OINT_Re#	8^3	7	11	LF	$3000, 1600, 800$
N7_OINT_HLLC_Re#	8^3	7	11	HLLC	$3000, 1600, 800$
N7_OINT_Roe_Re#	8^3	7	11	Roe	$3000, 1600, 800$
N3_OINT_Re#	16^3	3	5	LF	$\infty, 3000, 1600, 800$
N3_Re#	16^3	3	$--$	LF	$\infty, 3000, 1600, 800$

TABLE 1. Overview of all simulated TGV cases. The second column gives a total number of elements used, N is a polynomial order in individual elements, N_{Over} a polynomial order used for over integration, and employed numerical flux functions are indicated in column 'Flux'. Each case was run for several different Reynolds numbers indicated by Re# in the case name and listed in the last column.

CCM+ [22]. The initial conditions, following [23], are

$$u = u_0 \left[sin(x)cos(y)cos(z) \right], \tag{4.1}$$

$$v = -u_0 \left[cos(x)sin(y)cos(z) \right], \tag{4.2}$$

$$w = 0, \tag{4.3}$$

$$\rho = \rho_0, \tag{4.4}$$

$$p = p_0 + \frac{\rho_0}{16} \left[(cos(2x) + cos(2y))(cos(2z) + 2) - 2 \right], \tag{4.5}$$

where subscript $[\quad]_0$ indicates reference quantities. To obtain nearly incompressible results, the reference Mach number was set to $Ma = 0.1$. The initial flow field is let to evolve for 10 non-dimensional time units where the time unit is $T = l_0/u_0$ where $l_0 = 1$ is the reference length.

Numerical dissipation reference data is available for Reynolds numbers ranging from 100 to 3000, see e.g. [1, 22]. FLEXI simulations within this Reynolds number range and several numerical flux functions have been obtained. To maintain consistency with [1, 22] all FLEXI numerical simulations have been performed with 64^3 degrees of freedom (DoF). We vary the number of DG-Elements from 2^3 to 16^3 and the polynomial degree within each element along each spatial direction from 31 to 3. For the lowest polynomial degree, there are also results available with and without over integration, an overview of all cases is provided in Tab. 1.

With increasing Re, ε^n dominates over ε^{vis}. Focus is thus set on analysis of the case with $Re = 3000$.

4.1. *A numerical dissipation analysis of data interpolated to uniform meshes*

Within each element, the time-dependent FLEXI TGV simulation data is stored on a non-uniform mesh. However, the original method [1] was coded assuming data on uniform meshes. Therefore, to analyse the FLEXI TGV simulations we first interpolate the data, using oversampling, to a uniform mesh.

First we study the influence of the approximation order of fluxes for an estimate of the numerical dissipation. Figure 1 depicts ε^n for case $N3\_3000$ when local differences and cell-face interpolations in Eq. (2.9) are of approximation order 2 to 8. For fourth and sixth order approximations the results differ insignificantly. Higher-order approximations lead
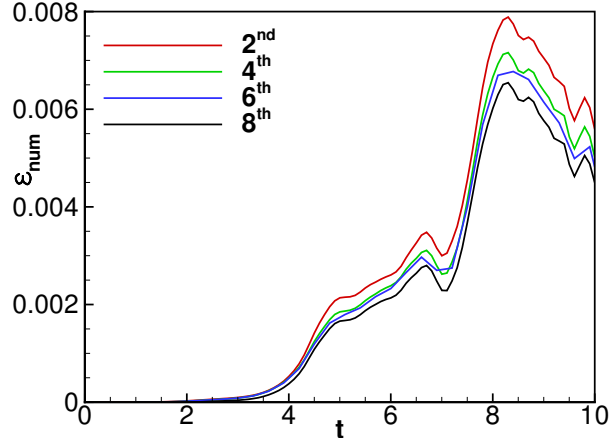
FIGURE 1. Numerical dissipation for different orders of approximation, case $N3\_3000$ with a uniform grid of 160^3 cells is shown.
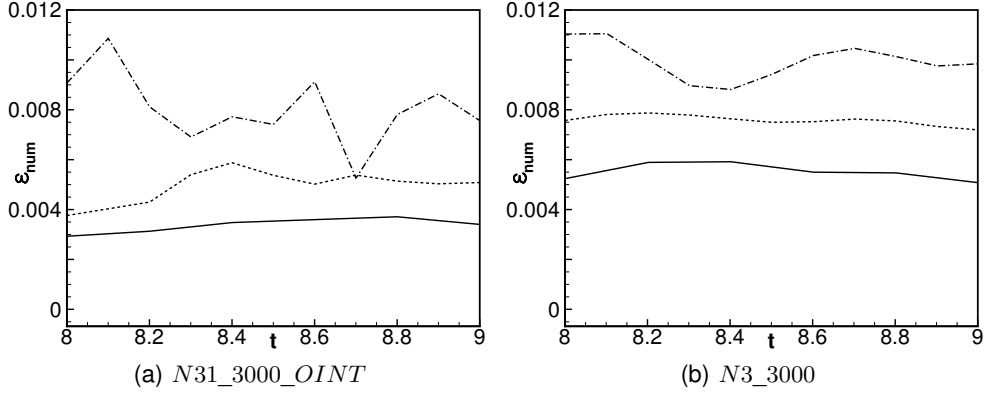

(a) $N31\_3000\_OINT$ (b) $N3\_3000$

FIGURE 2. Numerical dissipation rate within $8 \le t \le 9$. Results from uniform grids of 64^3 cells are indicated as (— · —), 128^3 as (– – – –), 256^3 as (———).

to $10 - 15\%$ (compared to 4th order) lower ε^n for $t \ge 8$; for other times the difference is lower than 5%. Yet, especially for finer grids, i.e. 256^3 cells or larger, the numerical cost for an 8th order approximation is signficantly larger than for an approximation order of four, which allows to provide a good estimate of the sought quantities. For coarser grids ε^n may be less accurate due to the less local stencils.

The dependence of estimates on oversampling is investigated by determining the convergence behavior for the two cases, $N31\_OINT\_3000$ and $N3\_3000$. Figs 2(a) and 2(b) show the $\varepsilon^n(t)$ for equispaced grids of 64^3, 128^3, 256^3 cells within the time frame of the dissipation peak ε^n. Interpolation to a larger number of equispaced cells is out of question due to the high demand of hard-disk space. Within this time frame we determine convergence rates, $p = ln\left(\frac{\varepsilon^n_{\Delta x_3} - \varepsilon^n_{\Delta x_2}}{\varepsilon^n_{\Delta x_2} - \varepsilon^n_{\Delta x_1}}\right) / \ln 2$, of $p_{E1} \approx 0.4$ and $p_{E2} \approx 0.6$ for when comparing the three grids. Further decrease of ε^n is expected for finer grids.

The procedure is further evaluated by comparing its results with results obtained for other simulations of the the same TGV flow. An equispaced post-processing grid with 160^3 cells has been chosen for comparisons with numerical dissipation rates and effec-
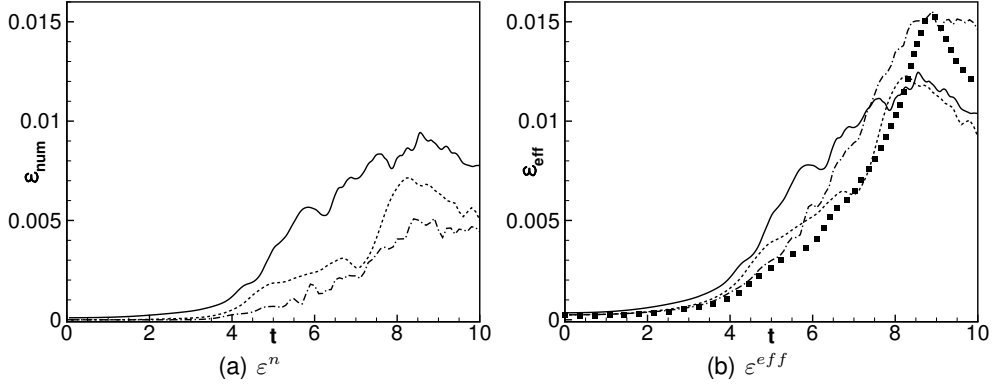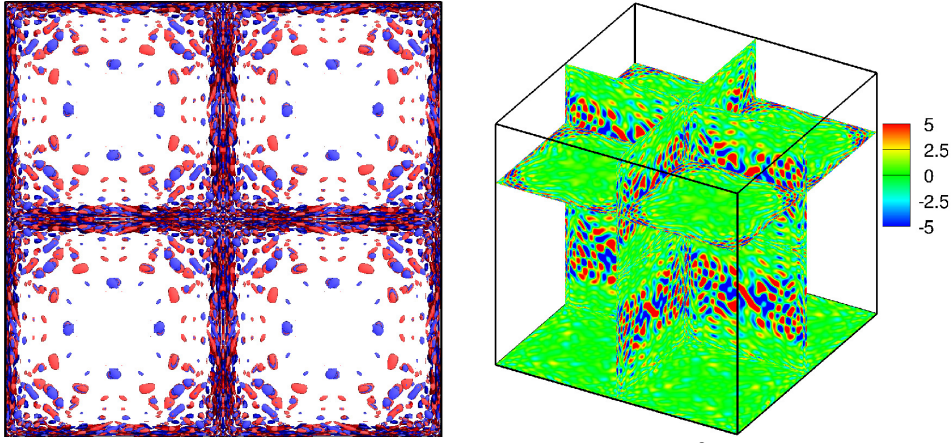
(a) ε^n

(b) ε^{eff}

FIGURE 3. ε^n and ε^{eff} for $N31\_OINT\_3000$ (—·—) and $N3\_3000$ (----) as compared to ALDM [1] (———), and DNS data of Brachet *et al.* (Symbols).

(a) Isosurfaces of positive and negative ε^n in x-y-plane (red: $\varepsilon^n = 4$, blue: $\varepsilon^n = -4$)

(b) 3-D view of $(2\pi)^3$ domain. Slices are at $z = -\pi$, $x = 0$, $y = 0$ and $z = 0.5\pi$.

FIGURE 4. Local numerical dissipation as identified on an equispaced grid of 256^3 cells at $t = 8.0$, case $N31\_OINT\_3000$.

tive dissipation rates of underresolved ALDM simulations with an equivalent number of DOF [1] and in DNS of Brachet *et al.* [24]. Compared to ALDM, the numerical dissipation as identified from the interpolated data is lower, see Fig. 3(a). Moreover, it correlates better with the onset of under-resolution, in a sense that there is a significant increase of ε^n at $t \approx 4$ while for earlier times it is negligible. Fewer elements, in conjunction with a larger polynomial degree, entail lower numerical dissipation rates, compare Fig. 3(a). Furthermore, $N31\_OINT\_3000$-data predictions for the peak ε^{eff} are closest to the DNS results. $\varepsilon^{eff}(t)$ for $0 \leq t \leq 8$ as identified from $N3\_3000$ data better approximates DNS $\varepsilon^{eff}(t)$ than ALDM predictions.

According to the numerical dissipation evaluation of the interpolated data, Fig. 4, ε^n concentrates at the element interfaces, while within the elements the contribution of ε^n to ε^{eff} is predicted to be negligible. Dissipative structures orient within the $x-y$ plane at $z \approx \pm\pi$ and are of a finite height in z-direction. Thereby, in each octant of the TGV these structures are point-reflection symmetric to the centre of the domain. Yet, in e.g. [1, 25]

three-dimensional, dissipative structures have been observed to spread more uniformly instead of focusing at the element boundaries as in fig. 4(b).

4.2. *A numerical dissipation analysis of data on DG meshes*

We want to compare the results obtained in section 4.1 with results taken directly from the DG code during runtime. In contrast to the post-processing method, the gradients obtained by the BR1 procedure are used for the calculations of the spatial terms in the kinetic energy equation. When the gradients are calculated from the solution variables, only the local gradients of the polynomial representation of the approximate solution can be recovered. They do not necessarily correspond to the lifted gradients that are used during the actual computation. Another difference lies in the fact that no reconstruction is used over the element boundaries, instead all terms are calculated on the discontinuous flow field and discontinuous gradient field that is obtained during the DG calculation.

4.2.1. *Integral analysis*

For a purely integral analysis in a periodic box, we can assume that only the viscous part of the spatial terms in Eq. (2.9) should have a non-zero contribution to the kinetic energy balance. This integral contribution is calculated following [26] as

$$\varepsilon^{vis} = \frac{2\nu}{8\pi^3} \iiint\limits_{0}^{2\pi} \frac{\partial u_i}{\partial x_j} \frac{\partial u_j}{\partial x_i} \, \mathrm{d}\mathbf{x}, \tag{4.6}$$

while the integral kinetic energy is taken as

$$E^{kin} = \frac{1}{16\pi^3} \iiint\limits_{0}^{2\pi} u_i u_i \, \mathrm{d}\mathbf{x}. \tag{4.7}$$

Figure 5 shows the temporal derivative of the kinetic energy and the numerical dissipation obtained by this method for different polynomial degrees and the TGV with both $Re = 3000$ and $Re = 800$. The results for $-\frac{dE^{kin}}{dt}$ are also compared to DNS data, taken from Fauconnnier *et al.* [27] for the $Re = 3000$ case, and from Brachet *et al.* [24, 28] for the $Re = 800$ and $Re = 1600$ cases. For the lower Reynolds number case, most simulations closely follow the DNS data. A significant amount of numerical dissipation is only observed for the lowest polynomial degree of $N = 3$. It is also worth noting that the $N = 31$ case departs from the reference solution at the late stages, a behaviour that could indicate some remaining aliasing effects not captured by the over integration. In practive, a polynomial degree as high as 31 would not be used. When the Reynolds number is increased, the simulations will become more and more underresolved and this should lead to an increase in numerical dissipation. This behaviour is verified in the results for the $Re = 3000$ TGV. Due to the higher resolution requirements, none of the simulations can exactly reproduce the DNS data. But again the calculations with the lowest polynomial degree suffer from the highest numerical dissipation.

4.2.2. *Local analysis*

To obtain local results for the numerical dissipation, the evaluation of all the spatial terms in Eq. (2.1) has been implemented in the DG code FLEXI. Since the evaluation of this equation demands knowledge of second derivatives, the BR1 method has been applied a second time to the gradients to get a consistent representation of the second derivatives in the DG context. To be able to validate the local results, the values are

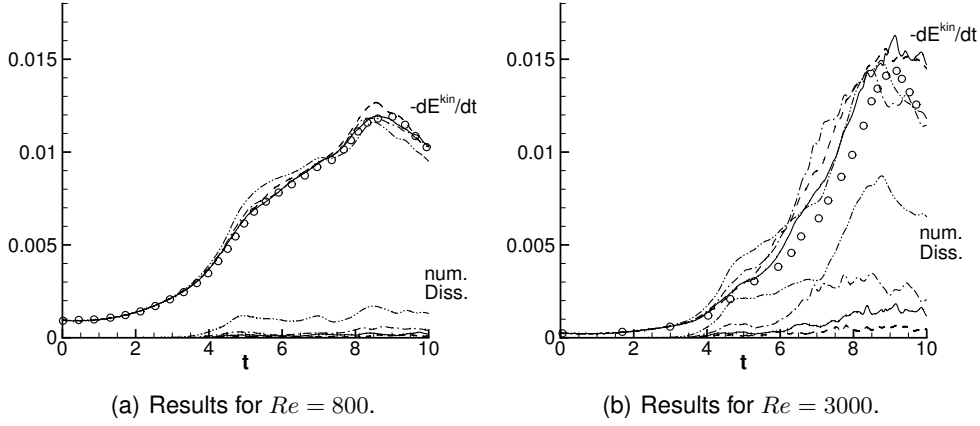(a) Results for $Re = 800$.　　　　　(b) Results for $Re = 3000$.

FIGURE 5. Integral results for numerical dissipation from evaluation of derivatives in DG code, considering only viscous dissipation. Upper curves show $-\frac{dE^{kin}}{dt}$, lower curves numerical dissipation. $----$ $N = 31$, ——— $N = 15$, —·— $N = 7$, —··— $N = 3$, ○ DNS (Brachet *et al.* [24], Fauconnier *et al.* [27]).

Case	ε^{vis} Eq. (4.6)	viscous Eq. (2.1)	pressure Eq. (2.1)	convection Eq. (2.1)	ε^n only viscous	ε^n all parts
N31_OINT_3000	$1.30 \cdot 10^{-2}$	$1.30 \cdot 10^{-2}$	$-1.86 \cdot 10^{-6}$	$1.61 \cdot 10^{-4}$	$3.90 \cdot 10^{-4}$	$2.36 \cdot 10^{-4}$
N15_OINT_3000	$1.09 \cdot 10^{-2}$	$1.09 \cdot 10^{-2}$	$-7.73 \cdot 10^{-6}$	$3.79 \cdot 10^{-4}$	$1.37 \cdot 10^{-3}$	$1.00 \cdot 10^{-3}$
N7_OINT_3000	$1.04 \cdot 10^{-2}$	$1.04 \cdot 10^{-2}$	$-3.13 \cdot 10^{-5}$	$5.71 \cdot 10^{-4}$	$1.80 \cdot 10^{-3}$	$1.27 \cdot 10^{-3}$
N3_OINT_3000	$5.99 \cdot 10^{-3}$	$5.98 \cdot 10^{-3}$	$-1.85 \cdot 10^{-5}$	$4.60 \cdot 10^{-4}$	$6.89 \cdot 10^{-3}$	$6.46 \cdot 10^{-3}$

TABLE 2. Comparison of integral numerical dissipation obtained by purely integral and local evaluations. Second column results for viscous dissipation obtained by Eq. (4.6), third column viscous dissipation from local evaluation of Eq. (2.1). Fourth and fifth column are pressure and convective term of Eq. (2.1), respectively. Last two columns numerical dissipation calculated only with viscous dissipation resp. with all parts of the kinetic energy balance. Evaluation at $t = 8$.

integrated over the whole domain and compared with the completely integral method in section 4.2.1. This comparison can be found for several polynomial degrees in Tab. 2 at a non-dimensional time of $t = 8$. It can be seen that the calculation of the viscous dissipation from Eq. (4.6) and from the viscous part of Eq. (2.1) yield the same results. Although the pressure and convection parts of Eq. (2.1) should be equal to zero in an analytical setting, they do have a contribution to the discrete kinetic energy balance. However, the viscous dissipation is the dominating factor in the evaluation of the numerical dissipation.

To compare the local results obtained in the DG code to the local results from the post-processing tool, Fig. 6 shows isosurfaces of the numerical dissipation from the evaluation in the DG code for a TGV computed with a polynomial degree of $N = 31$ and at a Reynolds number of $Re = 3000$. The same plot with results from the post-processing tool can be found in Fig. 4(a). The results for $t = 8$ show that by reconstructing over the discontinuous element boundaries the post-processing tool generates oscillations
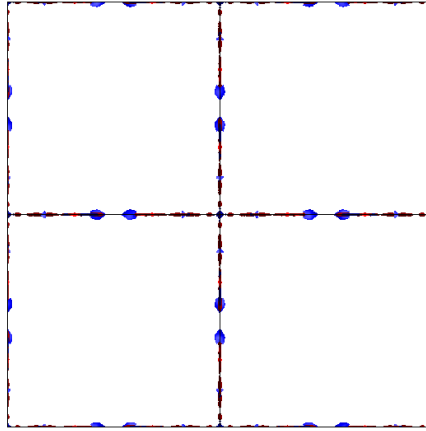
FIGURE 6. Local distribution of numerical dissipation for case N31_OINT_3000 at $t = 8$, top view. Isosurfaces of $\varepsilon^n = \pm 4$. Evaluation done in DG code.

originating at the element interfaces. While in the results obtained from the DG code high numerical dissipation is still centered around the boundaries, there is no oscillation visible.

5. Conclusions

The numerical dissipation rate in DG simulations of the Taylor-Green vortex flow has been estimated using the general technique of [1] implemented in two different ways. First, to be able to use the existing analysis tool restricted to data on uniform meshes the DG generated fields on nonuniform meshes were interpolated to uniform meshes with a number of grid points in each direction doubling from 64 through 128 to 256. For a fixed polynomial order N the computed numerical dissipation showed expected qualitative behavior of decreasing for increased resolution. However, because of a low convergence rate of the results with increasing interpolated mesh resolution we were not able to obtain firm quantitative results for all polynomial orders considered. While the numerical dissipation estimates for a low order $N = 3$ are consistent with the previous estimates for standard FV data the results for high order polynomials, in particular $N = 31$, are neither converged nor accurate. This led us to a second implementation of the procedure that used only the original DG data and the calculation of terms in definition (2.9) relying on high order numerical differentiations formulas used in the DG code itself. The numerical dissipation computed this way was comparable to that found using the interpolated data for $N = 3$ but was substantially less for higher polynomial orders N. To further clarify the origin of the observed differences a local analysis of the numerical dissipation was performed for the case $N = 31$. The analysis revealed that the main contribution to the numerical dissipation comes in both cases from the vicinity of elements' boundaries. However, the interpolation produces spurious oscillations with significant amplitudes near element interfaces, leading to inaccurate results for the numerical dissipation while the DG evaluation is free of these defects.

We conclude that for sufficiently high order N the DGSEM simulations are not affected significantly by the numerical dissipation effects. However, for the very low order

$N = 3$ the numerical dissipation in the DG method is comparable to that observed for standard FV codes and is not entirely negligible even for a slightly higher order $N = 7$. A secondary conclusion, based on our experience with the interpolated data, is that it is advisable and safer to implement the procedure for estimating the numerical dissipation using numerical formulas and discretizations from the analyzed code itself. Nevertheless, it is possible that simply avoiding an interpolation to uniform grids will produce accurate results. Therefore, we plan to extend the original, FV based analysis on uniform meshes of [1] to non-uniform meshes.

Acknowledgments

References

[1] SCHRANNER, F.S., DOMARADZKI, J.A., HICKEL, S., AND ADAMS, N.A.(2015). Assessing the numerical dissipation rate and viscosity in numerical simulations of fluid flows. *Comp. & Fluids*, **114**, 84–97.

[2] CASTIGLIONI, G., DOMARADZKI, J.A.(2015) A numerical dissipation rate and viscosity in flow simulations with realistic geometry using low-order compressible Navier–Stokes solvers. *Comp. & Fluids*, **119**, 37–46.

[3] BECK, A. D. AND BOLEMANN, T. AND FRANK, H. AND HINDENLANG, F. AND STAUDENMAIER, M. AND GASSNER, G. J. AND MUNZ, C.-D.(2013). Discontinuous Galerkin for High Performance Computational Fluid Dynamics. *High Performance Computing in Science and Engineering*. Springer, 281–294.

[4] POPE, S. B. (2000) *Turbulent flows*. Cambridge University Press.

[5] SAGAUT, P. (2006) *Large eddy simulation for incompressible flows: an introduction*, 3rd edn. Springer.

[6] GARNIER, E. AND ADAMS, N. AND SAGAUT, P. (2009). Large eddy simulation for compressible flows. Springer.

[7] BORIS, J.P. AND GRINSTEIN, F.F. AND ORAN, E.S. AND KOLBE, R.L. (1992). New insights into large eddy simulation. *Fluid Dyn. Res.* **10**, 199-228.

[8] GRINSTEIN, F., MARGOLIN, L. & RIDER, W. (2007). *Implicit Large Eddy Simulation: Computing Turbulent Flow*. Cambridge University Press.

[9] GARNIER, E., MOSSI, M., SAGAUT, P., COMTE, P., AND DEVILLE, M. (1999). On the use of shock-capturing schemes for large-eddy simulation. *J. Comp. Phys.* **153**, 273–311.

[10] DOMARADZKI, J. A., XIAO, Z., AND SMOLARKIEWICZ, P. K. (2003). Effective eddy viscosities in implicit large eddy simulations of turbulent flows. *Phys. Fluids* **15**, 3890–3893.

[11] DIAMESSIS, P.J., LIN, Y.C., AND DOMARADZKI, J.A. (2008). Effective numerical viscosity in spectral multidomain penalty method-based simulations of localized turbulence. *J. Comp. Phys.* **227**, 8145–8164.

[12] DOMARADZKI, J.A., RADHAKRISHNAN, S. (2005). Effective eddy viscosities in implicit modeling of decaying high Reynolds number turbulence with and without rotation. *Fluid Dyn. Res.* **36**, 385–406.

[13] KOPRIVA, D. A. (2006). Metric identities and the discontinuous spectral element method on curvilinear meshes. *Journal of Scientific Computing* **26**, 301–327.

[14] KOPRIVA, D. A. (2009). *Implementing Spectral Methods for Partial Differential Equations: Algorithms for Scientists and Engineers*, 1st ed. Springer Publishing Company, Incorporated.

[15] TORO, E. (1999). *Riemann Solvers and Numerical Methods for Fluid Dynamics*. Springer.

[16] BASSI, F. AND REBAY, S. (1997). A High Order Accurate Discontinuous Finite Element Method for the Numerical Solution of the Compressible Navier–Stokes Equations. *J. Comp. Phys.* **131**, 267–279

[17] CARPENTER, M., AND KENNEDY, C. (1994). Fourth-order 2N-storage Runge-Kutta schemes. *Tech. Rep.* NASA TM 109111.

[18] GASSNER, G., AND BECK, A. (2012). On the accuracy of high-order discretizations for underresolved turbulence simulations. *Theoretical and Computational Fluid Dynamics* **27**, 221–237.

[19] KIRBY, R., AND KARNIADAKIS, G. (2003). De-aliasing on non-uniform grids: algorithms and applications. *J. Comp. Phys.* **191** , 249–264.

[20] TAYLOR, G.I. AND GREEN, A.E. (1937). Mechanism of the production of small eddies from large ones. *Proc. R. Soc. Lond. A* **158**, 499–521.

[21] HICKEL, S., ADAMS, N.A., DOMARADZKI, J.A. (2006). An adaptive local deconvolution method for implicit LES. *J. of Comput. Phys.* **213**, 413–436.

[22] CASTIGLIONI, G., AND DOMARADZKI, J.A. (2015). On the evaluation of numerical dissipation rate and viscosity in commercial CFD code. *Proceedings of International Symposium on Turbulence and Shear Flow Phenomena 9*, Melbourne, paper 7B-1.

[23] SHU, C.-W., DON, W.-S., GOTTLIEB, D., SCHILLING, O., AND JAMESON, L. (2005). Numerical convergence study of nearly incompressible, inviscid Taylor–Green vortex flow. *J. Sci. Comp.* **24**.

[24] BRACHET, M.E. (1991). Direct simulation of three-dimensional turbulence in the Taylor-Green vortex. *Fluid Dyn. Res.* **8**, 1–8

[25] SCHRANNER, F.S., ROZOV, V., AND ADAMS, N.A. (2016). Optimization of an Implicit LES Method for Underresolved Simulations of Incompressible Flows *Proceedings of the 54th AIAA Aerospace Meeting*, San Diego, California.

[26] FAUCONNIER, D. (2008). *Development of a dynamic finite difference method for large-eddy simulation.* Dissertation, Ghent University, Belgium.

[27] FAUCONNIER, D., BOGEY, C., DICK, E. AND BAILLY, C. (2011). Assessment of large-eddy simulation based on relaxation filtering: application to the Taylor-Green vortex. *Proceedings of the Seventh International Symposium on Turbulence and Shear Flow Phenomena*, Ottawa, Canada.

[28] BRACHET, M.E., MEIRON, D.I., ORSZAG, S.A., NICKEL, B.G., MORF, R.H. AND FRISCH, U. (1983). Small-scale structure of the Taylor-Green vortex. *J. Fluid Mech.* **130**, 411–452.